



ELSEVIER

Nuclear Physics A 683 (2001) 3–20



www.elsevier.nl/locate/npe

Measurement of 42 MeV ${}^7\text{Li}$ projectile breakup on ${}^{208}\text{Pb}$ target near grazing incidence

Dhruba Gupta ^{a,*}, C. Samanta ^a, A. Chatterjee ^b, S. Kailas ^b, B.J. Roy ^b,
K. Mahata ^b, A. Shrivastava ^b

^a Saha Institute of Nuclear Physics, 1/AF, Bidhannagar, Calcutta 700064, India

^b Nuclear Physics Division, Bhabha Atomic Research Centre, Mumbai 400085, India

Received 13 April 2000; revised 24 July 2000; accepted 30 August 2000

Abstract

Breakup of 42 MeV ${}^7\text{Li}$ projectiles in the field of a ${}^{208}\text{Pb}$ target are studied near the grazing angle. In inclusive breakup measurements, angular distribution of the α and t fragments are found to be rather flat in nature. The α -t coincidence measurements are carried out with wide angular separations between the detected fragments. The choice of detection angles enables measurement in the same range of fragment relative energies but very different ${}^7\text{Li}^*$ scattering angles. The direct breakup contribution is found to dominate over the sequential breakup for the $\theta_\alpha > \theta_t$ set, while the reverse is true when $\theta_\alpha < \theta_t$. Calculations performed in a full quantum mechanical framework reproduce the overall shape of the direct breakup part of the present data and several existing data on ${}^{197}\text{Au}$ and ${}^{208}\text{Pb}$ targets at nearby energies. The sequential breakup is observed only from the decay of the 4.63 MeV ($7/2^-$) resonant excited state of ${}^7\text{Li}$ and its angular distribution does not fully agree with the existing theoretical predictions. Unlike the direct part, the sequential breakup cross section does not decrease with increasing scattering angles. Similar measurements with halo nuclei would be helpful to study their unknown resonant states. © 2001 Elsevier Science B.V. All rights reserved.

PACS: 25.70.Mn; 24.50.+g; 25.45.De; 25.60.Gc

Keywords: Nuclear reactions ${}^{208}\text{Pb}({}^7\text{Li}, {}^7\text{Li})$; Measured $\sigma(\theta)$; ${}^{208}\text{Pb}({}^7\text{Li}, \text{X})$; ${}^{208}\text{Pb}({}^7\text{Li}, \alpha\text{t})$; $E = 42$ MeV; Elastic, direct and sequential breakup

1. Introduction

In recent times, the breakup of loosely bound stable light nuclei, in the field of a target nucleus, has received much attention, but most of the works concentrated on low relative kinetic energies of the breakup fragments, by choosing appropriate detection angles [1–5].

* Corresponding author.

E-mail addresses: dhruba@hp1.saha.ernet.in (D. Gupta), chhanda@hp1.saha.ernet.in (C. Samanta).

Measurements at wide separation angle between the fragments (i.e., at high relative kinetic energies) are very few in number, mainly due to the difficulty in such low-yield experiments [6–9]. But such measurements are important in the overall understanding of the breakup mechanism. The loosely bound stable nucleus ${}^7\text{Li}$, possessing a predominant $\alpha + t$ cluster structure, is a good candidate as its breakup reaction studies would help to understand the breakup of the weakly bound unstable radioactive isotopes of ${}^7\text{Li}$ [10]. In fact, as the structure and the resonant excited states of ${}^7\text{Li}$ are well known [11], one can use the breakup data of ${}^7\text{Li}$ to test the existing theoretical formulations of breakup before these theories can be extended for the halo nuclei. The breakup of ${}^7\text{Li}$ has been widely studied with various targets. Some theoretical predictions for sequential breakup of 42 MeV ${}^7\text{Li}$ on ${}^{208}\text{Pb}$ target exist [12], but there had been no experimental data to confirm the said predictions. In this work we have studied both the direct and sequential breakup of 42 MeV ${}^7\text{Li}$ breakup on ${}^{208}\text{Pb}$ target as it would provide important guidelines for the existing theories.

An interesting aspect of the ${}^7\text{Li}$ breakup reactions is that the data at low relative kinetic energies (order of keV) are usually applied to deduce astrophysical information [3,5]. But, to carry this out, the reaction involved has to be a one-step Coulomb breakup process. It could be possible to suppress nuclear breakup by proper choice of bombarding energy and detection angle, but still coupling of the various reaction channels might hinder such studies. In this context, measurements in the same range of bombarding energies but at large relative kinetic energies (available from wide angle measurements) would be useful to gain insight into the overall reaction mechanism. Pertinently, the events in such measurements (wide α - t separation) originate either from ${}^7\text{Li}$ breakup via its high-lying particle unstable states or, the direct breakup of ${}^7\text{Li}$ into the α - t continuum followed by strong final-state interactions. A brief summary of the existing data is given below.

Breakup of ${}^7\text{Li}$ at 70 MeV (well above Coulomb barrier) on ${}^{12}\text{C}$ and ${}^{208}\text{Pb}$ targets was first carried out by Shotter et al. [1], to observe the transition from sequential to rapid nonsequential (i.e. direct) processes. The breakup fragments were detected at equal angles ($\theta_\alpha = \theta_t$) and it was found that direct breakup contribution dies out at larger angles. Similar “above Coulomb barrier” measurements to draw astrophysical information at very low relative energies (~ 0 –2 MeV) were carried out by Utsunomiya et al. [2,3,5]. They performed 63 and 42 MeV ${}^7\text{Li}$ breakup on several targets having a wide range of charge numbers. Wide-angle measurements of ${}^7\text{Li}$ breakup at 70 MeV incident energy using ${}^{12}\text{C}$ and ${}^{120}\text{Sn}$ targets were first reported by Yorkston et al. [6]. Though the width of the states and the angular resolution of the experimental system made the identification of the individual components very difficult, fragment yields were found to spread over a wider angular range than would be expected for sequential breakup of ${}^7\text{Li}$. These wide-angle yields were considered to arise from a rapid direct breakup of ${}^7\text{Li}$ in the nuclear field of the target and the final channel fragments are simply being deflected by the target nucleus.

Measurements above Coulomb barrier by Gazes et al. [7] and Mason et al. [8] include both direct and sequential breakup of 54 MeV ${}^7\text{Li}$ using ${}^{12}\text{C}$ and ${}^{197}\text{Au}$ targets. The breakup products were detected at small scattering angles ($\theta_\alpha \neq \theta_t$), less than the grazing angle. The E1 Coulomb breakup calculations underestimated, throughout, the direct breakup cross sections using ${}^{12}\text{C}$ target, implying the importance of nuclear breakup. For ${}^{197}\text{Au}$ target,

interestingly, a five fold change in the direct breakup yield was observed by interchanging the fragment detection angles. Also, the Coulomb breakup calculations satisfactorily reproduced the quasielastic direct breakup part except near grazing angle, attributable to nuclear absorption [8].

The wide use of polarized ${}^7\text{Li}$ beams at energies near and above Coulomb barrier to investigate the effects of ${}^7\text{Li} \rightarrow \alpha + t$ direct and sequential breakup, on the elastic scattering channel [13–17] deserves mention in this regard. Strong coupling of the elastic channel with various other channels is important near the Coulomb barrier. It is manifested in the appreciable effects of ${}^7\text{Li}$ projectile excitation (via bound excited state as well as unbound resonant and nonresonant continuum states) on the 33 MeV ${}^7\text{Li} + {}^{208}\text{Pb}$ elastic scattering differential cross section [15]. The studies also revealed a “threshold anomaly” (sudden and sharp variation of the potential near Coulomb barrier) in the central and tensor parts of the optical potential [18,19]. In fact studies in a coupled-channel framework have found that projectile excitation is a dominant effect in the vector analyzing power for elastic scattering [13]. For the ${}^7\text{Li} + {}^{58}\text{Ni}$ system at $E = 42$ MeV, the channel coupling effects on both the elastic scattering and sequential breakup have recently been studied [20], and it was found that although the channel coupling effects on the elastic channel are small, they are nonnegligible on the sequential channel. The channel coupling effects may however change if heavier targets are used [21,22].

The current work presents a wide-angle measurement of the 42 MeV ${}^7\text{Li}$ projectile breakup with ${}^{208}\text{Pb}$ target. Both the direct and sequential breakup contributions in the angular region near the grazing angle are investigated. At this incident energy (near but above the Coulomb barrier $E_c \sim 35$ MeV), the Coulomb breakup is expected to be dominating but, multi-step processes may contribute towards exciting the projectile into its continuum. Near Coulomb barrier, data are particularly suitable to study Coulomb–nuclear interference and any post Coulomb acceleration of the breakup fragments in the presence of a high- Z target like ${}^{208}\text{Pb}$. Prior DWBA calculations have been carried out to explain the direct breakup part of the spectra. To get a consistent picture, similar analysis of the existing data of ${}^7\text{Li}$ breakup at 63 MeV on ${}^{208}\text{Pb}$ [3] and 54 MeV on ${}^{197}\text{Au}$ [8] targets were performed, along with the comparison of the earlier work of 42 MeV ${}^7\text{Li}$ breakup on ${}^{58}\text{Ni}$ target [9]. Angular distribution of the sequential breakup data are presented and compared with the predictions of the existing coupled channel calculations of Sakuragi and Hirabayashi [12].

In the following sections we present the experimental details (Section 2), experimental data with analysis (Section 3) and a summary and conclusions (Section 4) of this work.

2. Experiment

The experiment was carried out with the 42 MeV ${}^7\text{Li}$ beam from the BARC-TIFR Pelletron at Mumbai. A self-supporting enriched ${}^{208}\text{Pb}$ target of thickness 2.0 mg/cm^2 was used. Three ΔE – E telescopes with Si ΔE and Si(Li) E -detectors (Fig. 1) were used for particle identification. Telescopes 1 and 3 ($\Delta E = 150 \text{ } \mu\text{eV}$, $E = 2 \text{ mm}$) were used to

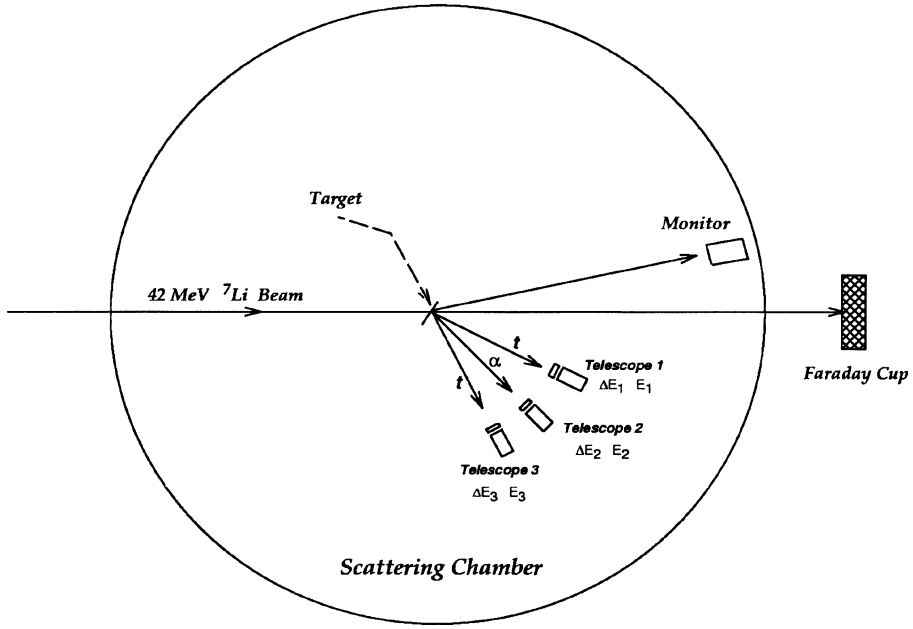


Fig. 1. Schematic diagram of the experimental setup.

detect d and t, while telescope 2 ($\Delta E = 50 \mu$, $E = 2 \text{ mm}$) to detect α , ${}^6\text{He}$, ${}^6\text{Li}$ and ${}^7\text{Li}$. The beam current was kept between 5–30 nA. The telescopes were mounted on two independent arms of a one meter diameter scattering chamber. Telescope 1 was placed in one arm while telescopes 2 and 3 in the other arm. Telescope 3 was kept fixed with respect to telescope 2 by a relative angular separation of 20° . While taking inclusive data both the arms have been rotated appropriately to get an angular distribution. During the exclusive measurements telescope 1 was kept at 30° while telescope 2 at 52° and hence telescope 3 at 72° near the grazing angle ($\theta_{\text{graz}} \sim 72^\circ$), where the elastic cross section normalized by the Rutherford cross section falls to ~ 0.25 . Two sets of coincident measurements were performed and the opening angles in this geometry are within the sequential cone of about 26° , for the ${}^7\text{Li}^* (4.63 \text{ MeV}) \rightarrow \alpha + t$ ($Q = 2.47 \text{ MeV}$) reaction. Wide-angle geometry resulted in the sequential peaks to arrive nearer to the beam velocity energy and thus cut off of any of them was avoided. Moreover, measurements at wide angles, in principle, provide opportunity to see breakup events of large α – t relative energy from higher resonant and nonresonant continuum states of ${}^7\text{Li}$. The minimum relative energy possible in this detector configuration can be seen from Fig. 2 in which the α – t relative energy ($E_{\alpha t}$) is plotted against the angle $\theta_{\text{cm}}({}^7\text{Li}^*)$, at which the excited ${}^7\text{Li}$ is scattered.

Standard electronics were used for the measurements and the data were stored in list mode for off-line analysis. The energy calibration was done by using a thorium alpha source [23] and also utilizing the ${}^7\text{Li}$ elastic peak. Due to small breakup cross sections at wide angular separations of the breakup fragments, the coincidence count rate was very low. However, the real to random ratio was quite high as can be seen from the TAC spectrum shown in Fig. 3.

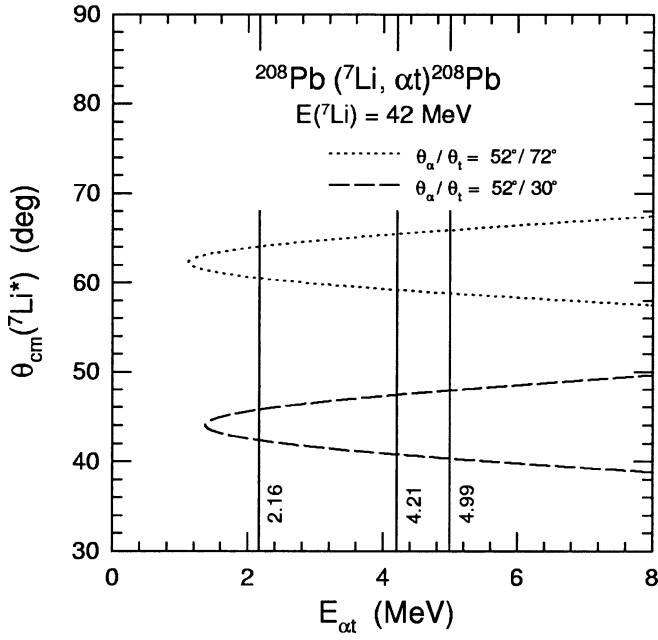


Fig. 2. The relative energy $E_{\alpha t}$ vs. $\theta_{cm}(^7\text{Li}^*)$ for the choice of angles in this work. The vertical lines signify the available relative energies in case of sequential decays via the resonant excited states of ^7Li .

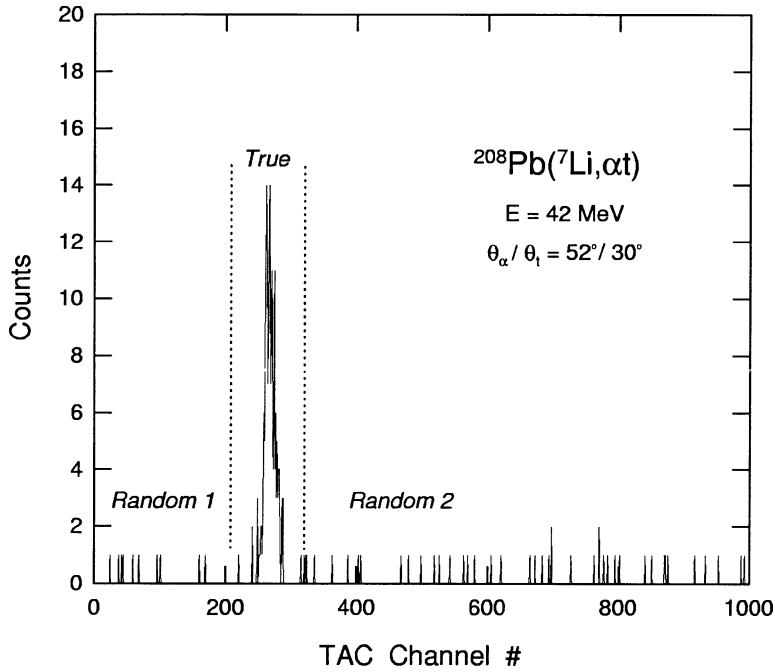


Fig. 3. The TAC spectra for the coincidence between α and t in the angular setup $\theta_\alpha/\theta_t = 52^\circ/30^\circ$.

3. Experimental data and analysis

The elastic angular distribution data from $^{208}\text{Pb}(^7\text{Li}, ^7\text{Li})$ scattering at $E(^7\text{Li}) = 42 \text{ MeV}$ is shown in Fig. 4. It is to be noted that the present ^7Li scattering data are really quasi-elastic in nature as the inelastic scattering to the ^7Li (0.478 MeV , $1/2^-$) state is not resolved in the experiment. However, in previous works of ^7Li scattering on ^{208}Pb target at nearby energies of 33 MeV [16], 63 MeV [3] and 68 MeV [24] the cross section of this state was found to be at most 10% of the elastic scattering at grazing angle and negligible at smaller angles. The data of the present work being inside grazing angle, the contribution of this state towards elastic scattering would be much less than 10%. The data were analyzed in a phenomenological optical model, using the code DWUCK4 [25]. The best fit optical potential parameters (Table 1) were obtained by a parametric search, starting from those of $52 \text{ MeV } ^7\text{Li}$ elastic scattering on ^{208}Pb target [26]. These best fit parameters were used in calculations of the direct breakup cross sections which will be explained later.

The kinetic energy of the incident ^7Li being appreciably larger than the binding energy of its constituents, breakup would play a significant role in its collision with a target. This was signalled by broad bumps in the continuum part of the inclusive energy spectra of the emitted particles d , t and α , shown at $\theta = 45^\circ$ (Fig. 5a). Basically these bumps are centered around their respective beam velocities, modulated by kinematics, Q -value and target loss. It is found that the α -bump is centered at a slightly higher and the t -bump at a slightly lower energy with respect to their respective beam velocity energies. This is explained by the Coulomb deceleration of the projectile in the entrance channel and

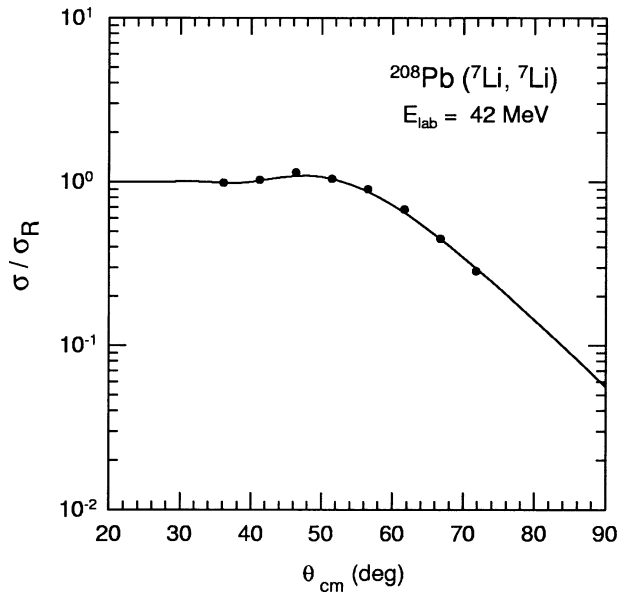


Fig. 4. The quasi-elastic scattering data of this work from $^7\text{Li} + ^{208}\text{Pb}$ collision, at $E(^7\text{Li}) = 42 \text{ MeV}$. The solid curve shows the phenomenological optical model calculations, the parameters of which are given in Table 1.

Table 1

Optical potential parameters used in this work $r_c = 1.40$ fm, $R_x = r_x A_T^{1/3}$

Reaction	E_{lab} (MeV)	V_o (MeV)	r_o (fm)	a_o (fm)	W_v (MeV)	r_I (fm)	a_I (fm)	Ref.
$^{208}\text{Pb}(^7\text{Li}, ^7\text{Li})$	63.0	244.0	1.450	0.650	12.00	1.680	0.900	[3]
$^{208}\text{Pb}(^7\text{Li}, ^7\text{Li})$	42.0	296.0	1.210	0.765	18.99	1.602	0.743	[*]
$^{208}\text{Pb}(\alpha, \alpha)$	36.0	37.8	1.220	0.570	2.00	1.220	0.570	[32]
$^{208}\text{Pb}(\alpha, \alpha)$	24.0	41.4	1.220	0.570	2.00	1.220	0.570	[32]
$^{208}\text{Pb}(t, t)$	27.0	163.4	1.160	0.769	13.90	1.442	0.864	[33]
$^{208}\text{Pb}(t, t)$	18.0	166.1	1.160	0.769	13.90	1.442	0.864	[33]
$^{197}\text{Au}(^7\text{Li}, ^7\text{Li})$	54.0	293.2	1.253	0.785	18.99	1.602	0.743	[26]
$^{197}\text{Au}(^7\text{Li}, ^7\text{Li})$	54.0	232.8	1.200	0.840	18.00	1.750	0.700	[30]
$^{197}\text{Au}(\alpha, \alpha)$	30.8	108.8	1.355	0.635	15.00	1.355	0.635	[34]
$^{197}\text{Au}(t, t)$	23.1	164.6	1.160	0.769	13.90	1.442	0.864	[33]

* This work.

the Coulomb acceleration of the fragments in the exit channel. The resultant energy of the fragment is expressed as $E_{\alpha/t} = \frac{A_{\alpha/t}}{A_{^7\text{Li}}} (E_{^7\text{Li}} - Z_{^7\text{Li}} V_c) + Z_{\alpha/t} V_c$, where $A(Z)$ is the mass (charge) number of the respective nuclei. Considering V_c (Coulomb energy/charge) ~ 10 MeV, we find that the shift in the α energies is about +2.8 MeV and for the tritons about -2.8 MeV, in agreement with the present data. Due to its strong binding energy, the alpha-particle remains as it is in reactions and the spectra shows appreciable number of them coming via compound nucleus formation. At a higher detection angle of $\theta = 70^\circ$ (Fig. 5b), the α -particles coming from an intermediate compound nucleus decrease considerably compared to breakup events and at this angle, the 2.61 MeV (3^-) excited state of ^{208}Pb is identified and shown in a magnified scale. The deuterons may be coming via ^6Li ($^7\text{Li} \rightarrow ^6\text{Li}^* [\rightarrow \alpha + d] + n$) breakup and are much lesser in yield compared to other particles. Discrete lines to low lying states in ^{209}Bi and ^{209}Pb are seen in the ^6He and ^6Li spectra respectively. The breakup part and the compound part in the spectra were separated from each other by appropriate peak fittings and the inclusive breakup cross sections are obtained by integrating the breakup contributions of the energy spectra. The resulting angular distributions for α and t are found to be very slowly falling (Fig. 6) showing a maxima at around 60° . Although in this angular region the elastic cross section falls by three orders of magnitude, variation of inclusive breakup cross sections is less than one order of magnitude. In comparison, the angular distributions of α and t inclusive breakup on a medium mass target ^{58}Ni , were forward peaked, and a steady decrease in cross section by two orders of magnitude was observed over the angular region 10° to 70° [9]. The reason is that for the ^{208}Pb target major part of the inclusive data resides within the grazing angle ($\sim 72^\circ$), while for ^{58}Ni , most of the data are outside the grazing angle ($\sim 27^\circ$). But in both cases the α -cross section is uniformly greater than the t-cross section, indicating possible absorption of tritons in target and/or, more channels for production of α -particles other than $^7\text{Li} \rightarrow \alpha + t$ breakup.

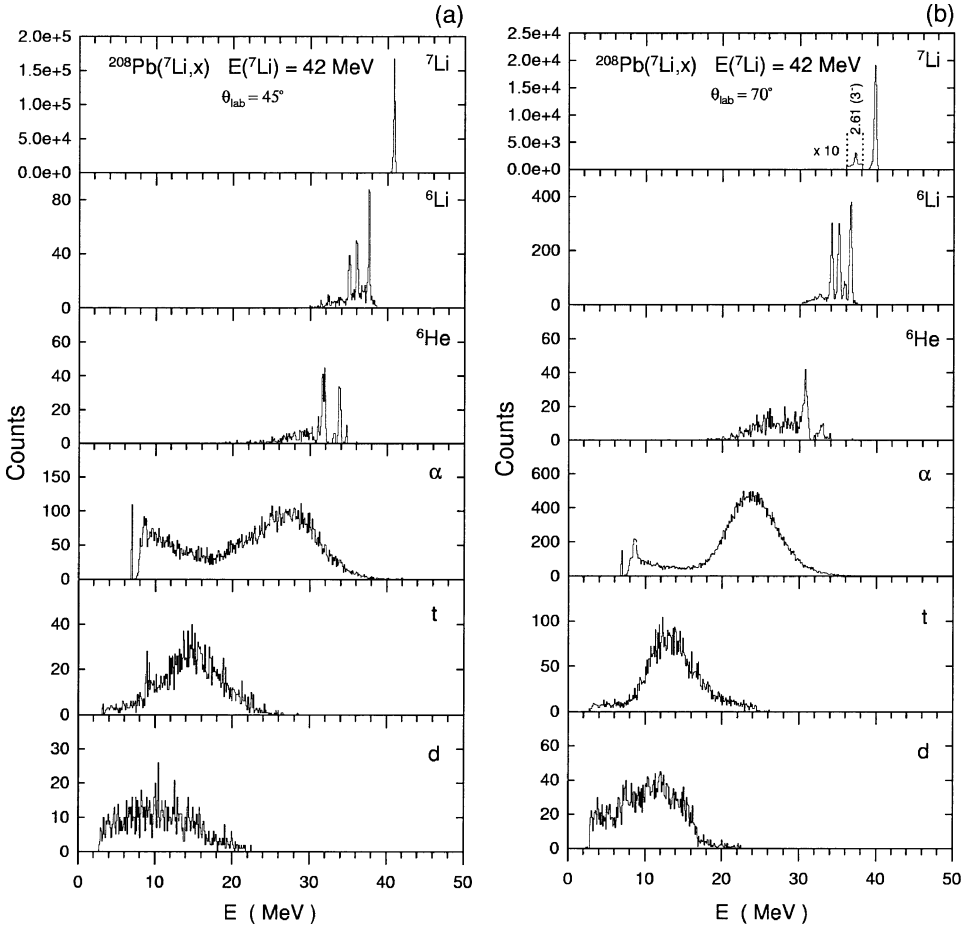


Fig. 5. The inclusive spectra in $^{208}\text{Pb}(^7\text{Li}, x)$ reaction for $E(^7\text{Li}) = 42$ MeV at (a) $\theta = 45^\circ$, and (b) $\theta = 70^\circ$, where $x = d, t, \alpha, ^6\text{He}, ^6\text{Li}$ and ^7Li . The 2.61 MeV (3^-) excited state of ^{208}Pb is shown in a magnified scale in (b).

During α - t coincidence measurements, events of about the same range of relative energies between the breakup fragments (Fig. 2) but originating from projectiles scattered at widely different angles [$\theta_{\text{cm}}(^7\text{Li}^*)$] were recorded. Two sets of coincidence data were obtained from three sets of ΔE - E telescopes. Thus for one set $\theta_\alpha (52^\circ) > \theta_t (30^\circ)$ and for the other set $\theta_\alpha (52^\circ) < \theta_t (72^\circ)$. The α - t separation angle ($\sim 20^\circ$) being less than the sequential cone angle ($\sim 26^\circ$) for resonant breakup of ^7Li (via the 4.63 MeV [$7/2^-$] state), the sequential decays were observed in both the detector geometries. The expected positions of the peaks are indicated by arrows in the triton energy spectra (Fig. 7). They agree with the locations of the observed peaks, but a prominent asymmetry can be seen in the yields of the two sequential peaks. The high-energy tritons (low-energy α -particles) are found to be more in numbers than the low-energy tritons (high-energy α -particles), largely apparent for the detector geometry $\theta_\alpha < \theta_t$. Eventually, in both the geometries the

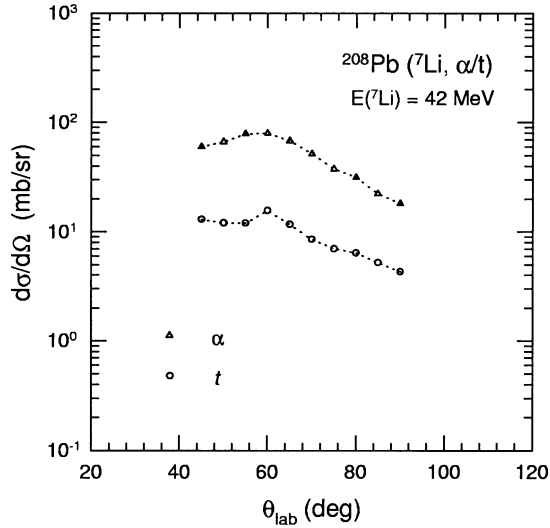


Fig. 6. The angular distributions of the inclusive breakup cross sections of α and t (in the lab frame) from 42 MeV ${}^7\text{Li} + {}^{208}\text{Pb}$ scattering. The dotted curves are guides to the eyes.

Table 2

The center of mass angles of ${}^7\text{Li}^*$ and α, t fragment energies in sequential breakup

θ_α/θ_t (deg/deg)	E_t (MeV)	E_α (MeV)	$\theta_{\text{cm}}({}^7\text{Li}^*)$ (deg)
$52^\circ/30^\circ$	10.5	27.5	45.5
$52^\circ/30^\circ$	22.0	16.5	42.5
$52^\circ/72^\circ$	10.0	28.0	60.5
$52^\circ/72^\circ$	22.5	15.5	64.0

low-energy triton yield essentially remains the same, whereas the high-energy triton yield is enhanced by about a factor of three for the $\theta_\alpha < \theta_t$ set. It is to be noted that in the present setup (unlike the work of Mason et al. [8]), the number of incident ${}^7\text{Li}$ projectiles are same in both $\theta_\alpha > \theta_t$ and $\theta_\alpha < \theta_t$ configurations; the data at both the angle pairs being taken simultaneously. The spectra also reflects that there is virtually no contribution from the nearby resonant excited or nonresonant continuum states above the 4.63 MeV state.

In the sequential decay picture, the ${}^7\text{Li}$ nucleus while passing near the target nucleus gets excited to a resonant state of finite lifetime. When the ${}^7\text{Li}^*$ decays, the α -particles and tritons come out in opposite directions in the rest frame of ${}^7\text{Li}^*$ (4.63 MeV, $7/2^-$). Two sharp peaks arise in the coincidence spectra at a particular θ_α/θ_t from two nearby angles of scattered ${}^7\text{Li}^*$, which satisfy the kinematic conditions. For the angular setups in this work, the possible ${}^7\text{Li}^*$ angles are given in Table 2 and also depicted in Fig. 7. The vector addition of the fragment velocities in their center of mass with the scattered ${}^7\text{Li}^*$ velocities results in high and low-energy tritons (or α -particles). The tritons which are moving forward in the α - t center of mass appear as the high-energy sequential peak in the triton spectra. Those

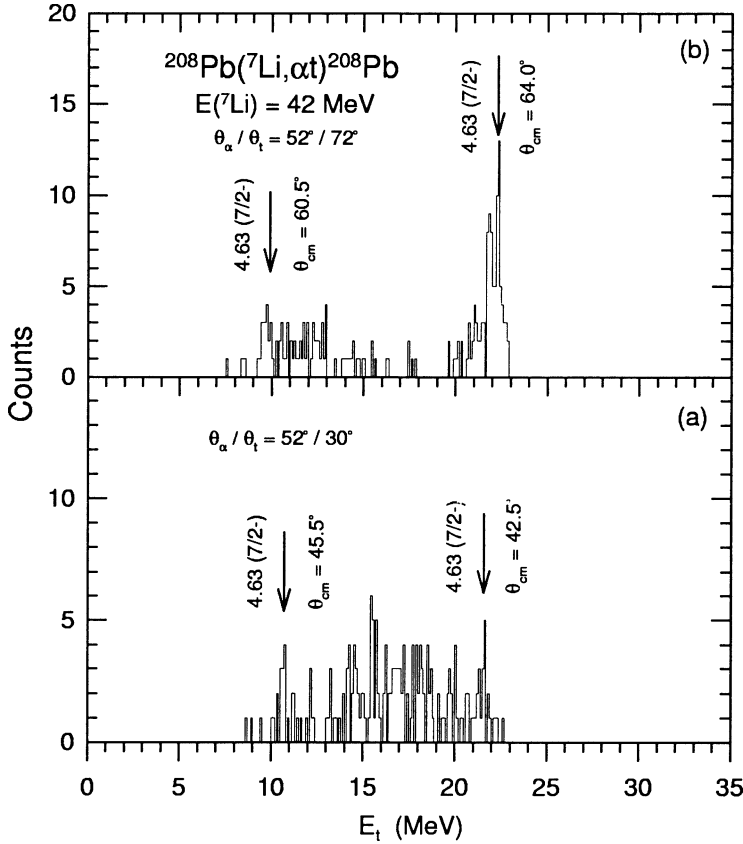


Fig. 7. The coincident triton energy spectra in 42 MeV $^{208}\text{Pb}(^7\text{Li}, \alpha t)^{208}\text{Pb}$ reaction at (a) $\theta_\alpha/\theta_t = 52^\circ/30^\circ$ and (b) $\theta_\alpha/\theta_t = 52^\circ/72^\circ$. The expected sequential peak positions are indicated by arrows and the center of mass angles of $^7\text{Li}^*$ corresponding to the sequential breakup peaks are also shown.

emitted in the backward direction appear as the low-energy peak. For the angular position $\theta_\alpha/\theta_t = 52^\circ/30^\circ$, the direct breakup contribution is found to be dominating compared to the sequential breakup (Fig. 7). At $\theta_\alpha/\theta_t = 52^\circ/72^\circ$, the direct breakup part attenuates and the high-energy tritons from sequential breakup increases by about three folds. The difference between θ_α and θ_t though remaining almost the same ($|\theta_\alpha - \theta_t| \sim 20^\circ$) in these two geometries, the $\theta_{\text{cm}}(^7\text{Li}^*)$ changes by about 20° (Table 2).

To explain the direct breakup part in the α -t coincidence spectra, theoretical calculations were performed in the prior-form DWBA formalism [27] where, in principle, all the final state interactions are taken into account except recombination [28,29]. It may be noted that, previous calculations [9] could successfully reproduce the shape of the low relative energy direct breakup spectra of 42 MeV ^7Li on ^{58}Ni ($\theta_\alpha = \theta_t = 10^\circ$) and 63 MeV ^7Li on ^{208}Pb ($\theta_\alpha = \theta_t = 15^\circ$) targets [9]. To get a consistent picture, the existing 54 MeV ^7Li breakup data (higher fragment relative energy) of Mason et al. [8] on ^{197}Au target were analyzed (Fig. 8) in the same framework [27]. The detection geometry in [8] was such

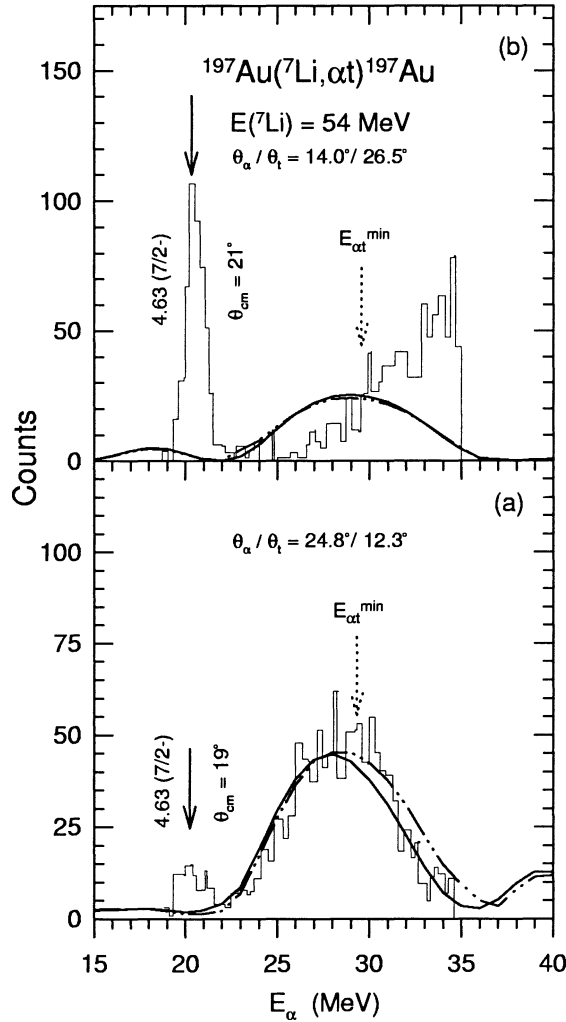


Fig. 8. The experimental data of ${}^7\text{Li}$ breakup, with ${}^{197}\text{Au}$ target at $E({}^7\text{Li}) = 54$ MeV [8] for (a) $\theta_\alpha / \theta_t = 24.8^\circ / 12.3^\circ$ and (b) $\theta_\alpha / \theta_t = 14.0^\circ / 26.5^\circ$. The solid (dash-dot-dotted) curves show the Coulomb + nuclear calculations in the prior-form DWBA framework (see text), employing the ${}^7\text{Li} + {}^{208}\text{Pb}$ (${}^6\text{Li} + {}^{197}\text{Au}$) OM parameters. The calculations are normalized to the experimentally observed direct breakup yields.

that the θ_α and θ_t positions were almost interchanged in two sets of measurements keeping $|\theta_\alpha - \theta_t|$ nearly constant, implying that the events recorded were those of ${}^7\text{Li}^*$ scattered at nearly constant angle. In addition, for the sake of completeness, analysis of the existing (low fragment relative energy) 63 MeV ${}^7\text{Li}$ direct breakup data ($\theta_\alpha = \theta_t = 20^\circ$) on ${}^{208}\text{Pb}$ target [3] was also carried out. In prior-form DWBA calculations [27–29] one needs optical model (OM) potential parameters as inputs. In the absence of best fit OM parameters for elastic scattering of ${}^7\text{Li}$ on ${}^{197}\text{Au}$ at 54 MeV, two sets of OM parameters (Table 1) at nearby energies were employed in the calculations, namely those of elastic scattering of 52 MeV

${}^7\text{Li} + {}^{208}\text{Pb}$ [26] and 30 MeV ${}^6\text{Li} + {}^{197}\text{Au}$ [30], with the real potential depths accordingly adjusted for 54 MeV incident energy. The required OM parameters of α and t scattering with the respective targets at the relevant energies are also given in Table 1. For the OM parameters of elastic scattering of t + ${}^{197}\text{Au}$ target, the corresponding t + ${}^{208}\text{Pb}$ elastic scattering OM parameters have been used. These calculations are depicted by the solid and dash-dot-dotted curves in Fig. 8, delineating minor change in shape with variation of OM potentials used here. In Ref. [8] the shape of the spectra were satisfactorily explained by classical Coulomb trajectory calculations. The E1 Coulomb breakup results reproduced the breakup cross sections except near the grazing angle. Thus the present quantum mechanical calculations are useful. The shape of the direct breakup part is reproduced for the $\theta_\alpha > \theta_t$ geometry (Fig. 8a). Here, the direct breakup yield delineates a maximum in the region of minimum relative energy ($E_{\alpha t} \sim 0.6$ MeV) of the emitted fragments. The calculations for the $\theta_\alpha < \theta_t$ geometry also show a maximum at minimum $E_{\alpha t}$ (~ 0.6 MeV) but, clearly the low-energy direct breakup α -particles ($E_\alpha < 30$ MeV) are depleted and the prior form results do not fully reproduce this observed asymmetry.

The coincidence spectra from the breakup of 63 MeV ${}^7\text{Li}$ with ${}^{208}\text{Pb}$ target at $\theta_\alpha = \theta_t = 20^\circ$, contains the unique situation of zero relative energy ($E_{\alpha t}^{\min} = 0$) between the detected fragments [3]. In Fig. 9, a and b, we show both the t and α coincident spectra and the relevant prior form calculations. To appreciate the contributions from the nuclear and Coulomb forces separately, the nuclear only and Coulomb only calculations are also shown by the dashed and dotted curves, respectively, showing the predominance of Coulomb breakup in this angular region. All the calculations in Fig. 9 have identical normalization factors. The coincident yield is minimum at $E_{\alpha t}^{\min} (\sim 0)$, as expected. Earlier [3] the yield minima was located by a quadratic power law fitting and the result was compared to the minima found from calculations in which the Coulomb effects were taken as zero. From this it was concluded that the fragments α and t do not suffer any strong post Coulomb acceleration. But this stability of relative energy minimum can also arise from the α -t interaction, and therefore not a good measure of final-state interaction with the target [8]. In our full quantum mechanical calculations, the low-energy part ($E_t < 26$ MeV) of the t-energy spectrum (Fig. 9a) is successfully reproduced, but the higher-energy part ($E_t > 26$ MeV) show that the experimental data is somewhat shifted towards lower energies compared to the theoretical predictions. However in the α -energy spectrum (Fig. 9b), the data have an overall shift towards lower energy, which was not so apparent in the earlier work over a wider α -energy range [9]. But the disagreement of the theoretical calculations with the experimental data is not so severe at this low α -t relative energy detection geometry, as compared to the above breakup data on ${}^{197}\text{Au}$ target.

The present work of 42 MeV ${}^7\text{Li}$ breakup with wide α -t separation angles using ${}^{208}\text{Pb}$ target is aimed at observing events of nearly same range of fragment relative energies but different ${}^7\text{Li}^*$ scattering angles by choosing appropriate geometry. The yield being low in such geometries, two sets of coincidence measurements were performed simultaneously from three sets of telescopes. Prominent direct breakup events (direct breakup being maximum around $E_{\alpha t}^{\min} \sim 1.4$ MeV, Fig. 10a) are observed for the $\theta_\alpha > \theta_t$ set, with very little contribution from sequential breakup events, but still an asymmetry signature in the

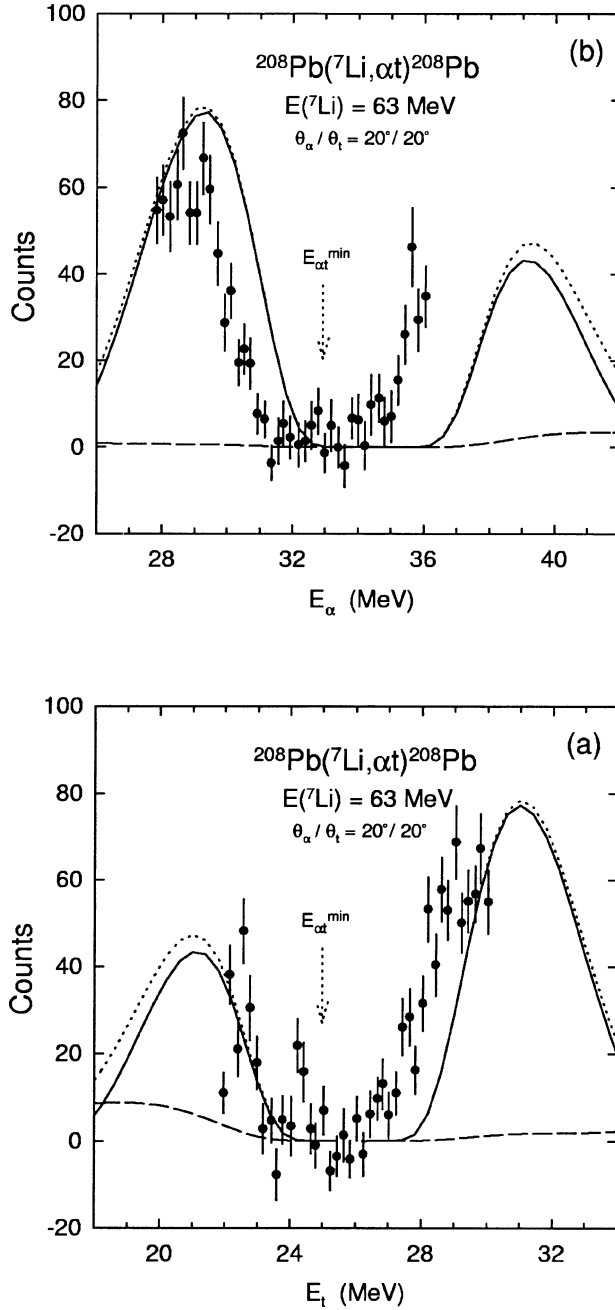


Fig. 9. The experimental data of ${}^7\text{Li}$ breakup, with ${}^{208}\text{Pb}$ target at $E({}^7\text{Li}) = 63 \text{ MeV}$ [3] for $\theta_\alpha = \theta_t = 20^\circ$. In the (a) triton and (b) α spectra, the solid curves show the Coulomb + nuclear calculations in the prior-form DWBA framework (see text). The nuclear (Coulomb) calculations separately are shown by the dashed (dotted) curves. The calculations are normalized by the same factor.

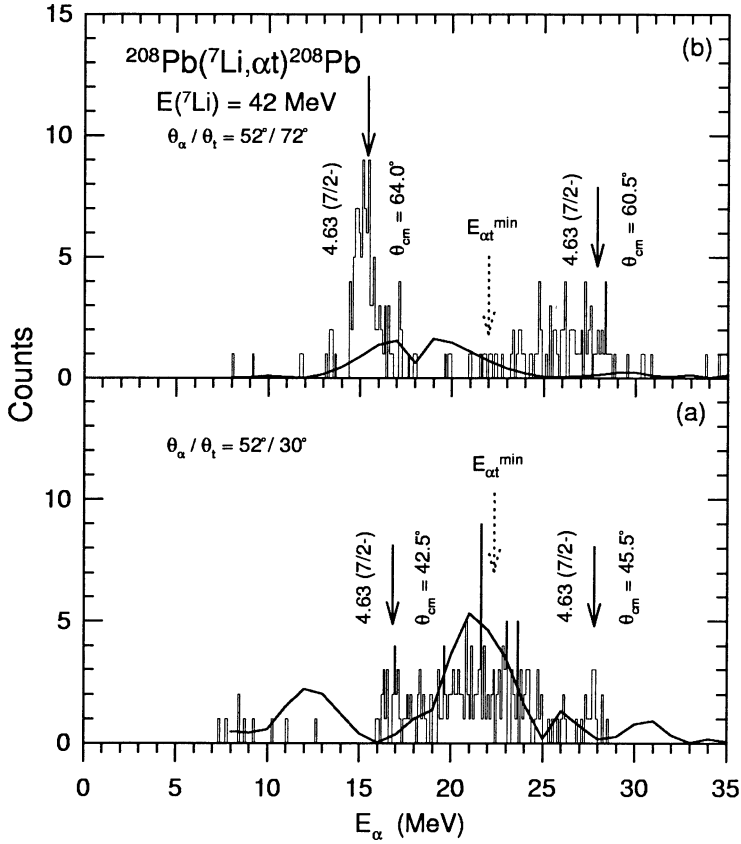


Fig. 10. The experimental data of ${}^7\text{Li}$ breakup, with ${}^{208}\text{Pb}$ target at $E({}^7\text{Li}) = 42$ MeV for (a) $\theta_\alpha / \theta_t = 52^\circ / 30^\circ$ and (b) $\theta_\alpha / \theta_t = 52^\circ / 72^\circ$. The solid curves show the Coulomb + nuclear calculations in the prior-form DWBA framework (see text). The calculations are shown normalized to the experimentally observed direct breakup yields.

two sequential peaks is apparent. For $\theta_\alpha < \theta_t$ and with increased ${}^7\text{Li}^*$ scattering angle, low-energy α particles from sequential decay increase by about three folds, while direct breakup is highly suppressed at $E_{\alpha}^{\min} \sim 1.2$ MeV (Fig. 10b). The prior-form calculations satisfactorily reproduce the shape of the α -energy spectra (Fig. 10a). In Fig. 10b, the sequential peak at around 28 MeV could not be cleanly separated owing to contaminations from direct breakup. For the $\theta_\alpha < \theta_t$ detector geometry, the prior-form calculations do not agree with the observed α -particle yields at energies $E \geq 20$ MeV. It may be noted that, although the yield of the 0.48 MeV excited state of ${}^7\text{Li}$ is small compared to the elastic channel, it may have some coupling effect on the elastic channel. Effect of such coupling was investigated at 33 MeV incident energy (Fig. 9 of Ref. [16]), which was found to be small within the grazing angle. We have extracted the optical potential from our data, which were taken within the grazing angle. This potential is used in the subsequent direct breakup calculations. Variation of 10% of this potential does not have any significant effect on the results.

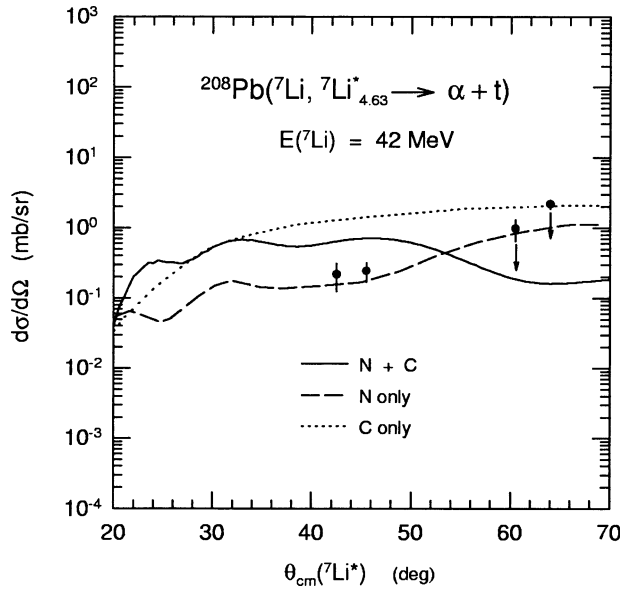


Fig. 11. The inelastic angular distribution data of this work from the $^{208}\text{Pb}(^7\text{Li}, ^7\text{Li}^*[4.63 \text{ MeV}] \rightarrow \alpha + t)$ reaction, at $E(^7\text{Li}) = 42 \text{ MeV}$. The solid curve shows the CDCC calculations incorporating both the Coulomb and nuclear interactions [12]. The dashed (dotted) curve depicts the CDCC calculations considering only the nuclear (Coulomb) interaction. The arrows indicate that the experimental cross sections shown in the angular region 60° – 70° reflect the upper limits only.

In earlier works, continuum discretized coupled channels (CDCC) calculations were found to provide good description of elastic and inelastic scattering of ^7Li [12,17,20,21]. Coupling to the first excited 0.48 MeV state was found to be important. Differential cross sections for sequential breakup of 70 MeV ^7Li via 4.63 MeV ($7/2^-$) state, with ^{120}Sn target have shown excellent agreement with the CDCC calculations (normalized by 0.584). Sequential breakup data for the $^7\text{Li} + ^{58}\text{Ni}$ system at 42 MeV incident energy is also found to agree very well with the coupled channel calculations [20]. In this work, the 0.48 MeV excited state of ^7Li could not be separated from the elastic peak. However, the 4.63 MeV ($7/2^-$) state could be clearly identified through breakup and the experimental sequential breakup cross sections were computed from the coincidence spectra, assuming isotropic emission of the breakup fragments in the frame of $^7\text{Li}^*$. The data are compared with the existing CDCC results of Sakuragi and Hirabayashi [12,31]. In Ref. [12], the nuclear wave function of ^7Li in the bound and unbound states were calculated by a microscopic $\alpha + t$ cluster model and the $\alpha + t + \text{target}$ three-body dynamics were treated in the framework of CDCC. The model space incorporates the g.s. ($3/2^-$), 0.478 MeV ($1/2^-$) state, as well as the P -wave ($l = 1$) and F -wave ($l = 3$) continuum, the F -wave continuum having a resonance in the 4.63 MeV ($7/2^-$) state. The experimental sequential breakup cross sections via the 4.63 MeV ($7/2^-$) resonant state along with the CDCC results (solid curve) of Ref. [12] are shown in Fig. 11. It is interesting to observe that although the fit is not very

good, the overall magnitude of the experimental cross sections is close to the theoretical predictions of Ref. [12] except at angles near the grazing angle. The data points in the 60° to 70° angular range represent only upper limits of the respective cross sections, as the direct breakup contributions here could not be separately accurately. The calculations of Ref. [12] incorporating separately the nuclear and the Coulomb parts are shown by the dashed and dotted curves, respectively, and this theory predicts considerable Coulomb–nuclear interference in the region of interest. Interestingly, the sequential breakup cross sections do not decrease in the angular region considered. The large sequential and low direct breakup contributions make the angles near grazing incidence suitable for identification of resonant states of nuclei. Thus such wide angle measurements would be useful for studying the halo nuclei, whose excited states are not well known.

4. Summary and conclusions

The present work encompasses the measurement of both direct and sequential breakup of 42 MeV ^7Li with ^{208}Pb target. The fragments α and t were detected at large angles with wide angular separations and thus high relative energy between them. The 42 MeV incident energy was chosen to be near but, above the Coulomb barrier ($E_c \sim 35$ MeV). Coupling of elastic to other channels and Coulomb–nuclear interference effects have been predicted earlier to be important at these energies. Although some theoretical predictions exist [12] for the 42 MeV $^7\text{Li} + ^{208}\text{Pb}$ sequential breakup cross sections, no experimental data for 42 MeV ^7Li breakup exist with the ^{208}Pb target.

The measurements of breakup cross sections are done inside the grazing angle and the inclusive α and t angular distributions are found to have maxima at around 60° , but compared to $^7\text{Li} + ^{58}\text{Ni}$ scattering [9] for which data were taken beyond grazing angle, the present angular distributions fall rather slowly. Both for the ^{58}Ni [9] and ^{208}Pb targets the inclusive α -cross sections are higher than the inclusive t -cross sections, implying more reaction channels for production of α -particles than tritons and possibly higher absorption of tritons in the targets.

Coincidence measurements were carried out for both $\theta_\alpha (52^\circ) > \theta_t (30^\circ)$ and $\theta_\alpha (52^\circ) < \theta_t (72^\circ)$ geometry. The two different geometry correspond to similar range of relative fragment energies but $^7\text{Li}^*$ scattering angle around 45° and 65° within the grazing angle (72°). For $\theta_\alpha > \theta_t$, the sequential breakup contributions from the 4.63 MeV ($7/2^-$) state of ^7Li is small compared to direct breakup, while the reverse is true for $\theta_\alpha < \theta_t$. Also, the high-energy t (low-energy α) coming from sequential breakup at $\theta_\alpha < \theta_t$ becomes appreciably large in numbers compared to their low-energy t (high-energy α) counterparts. The previously published CDCC calculations of Sakuragi and Hirabayashi [12] do not give the exact magnitude of the sequential cross sections, indicating scope for further improvement in various approximations used in the theoretical calculations.

The direct breakup data were analyzed in a full quantum mechanical framework (prior form DWBA). Analyses were done for both low and high relative energy fragments, which include 63 MeV [3] and 42 MeV ^7Li breakup on ^{208}Pb target, and the 54 MeV ^7Li breakup

on ^{197}Au target [7,8]. In the calculations, both the Coulomb and the nuclear breakup have been treated on equal footing, explicitly taking into account the Coulomb–nuclear interference. The α -particles and the high-energy tritons from the 63 MeV ^7Li breakup on ^{208}Pb (low relative energy fragments, less than 0.5 MeV including zero) are shifted towards lower energies compared to prior form predictions; in contrast to earlier predictions [5]. The disagreement of the theoretical results with the $\theta_\alpha < \theta_t$ 54 MeV breakup data (high relative energy greater than 0.6 MeV) on ^{197}Au is more severe for $E_\alpha < 30$ MeV, although successfully reproducing the $\theta_\alpha > \theta_t$ coincidence data.

At 42 MeV, with ^{208}Pb target the prior form DWBA calculations satisfactorily reproduced the data for the $\theta_\alpha > \theta_t$ geometry. However for $\theta_\alpha < \theta_t$ the exclusive data indicates necessity of improved theoretical calculations, which is beyond the scope of this work. Unlike the direct part, the sequential cross sections from resonant state do not diminish with angle appreciably. Such wide angle studies involving unstable halo nuclei would be very useful as controversies exist regarding their resonant states.

Acknowledgements

The authors thank all the BARC-TIFR Pelletron personnel for their kind assistance during the experiment and the VECC detector lab for providing the necessary detectors. The authors also thank Y. Hirabayashi for sending the results of his CDCC calculations of Ref. [12] in a tabular form. D.G. acknowledges CSIR, India, for financial support.

References

- [1] A.C. Shotter, A.N. Bice, J.M. Wouters, W.D. Rae, J. Cerny, Phys. Rev. Lett. 46 (1981) 12.
- [2] H. Utsunomiya, R.P. Schmitt, Y.-W. Lui, D.R. Haenni, H. Dejbakhsh, L. Cooke, P. Heimberg, A. Ray, T. Tamura, T. Udagawa, Phys. Lett. B 211 (1988) 24.
- [3] H. Utsunomiya, Y.-W. Lui, L. Cooke, H. Dejbakhsh, D.R. Haenni, P. Heimberg, A. Ray, B.K. Srivastava, R.P. Schmitt, T. Udagawa, Nucl. Phys. A 511 (1990) 379.
- [4] H. Utsunomiya, Y.-W. Lui, D.R. Haenni, H. Dejbakhsh, L. Cooke, B.K. Srivastava, W. Turmel, D. O'Kelly, R.P. Schmitt, D. Shapira, J. Gomez del Campo, A. Ray, T. Udagawa, Phys. Rev. Lett. 65 (1990) 847.
- [5] H. Utsunomiya, Y. Tokimoto, H. Mabuchi, K. Osada, T. Yamagata, M. Ohta, Y. Aoki, K. Hirota, K. Ieki, Y. Iwata, K. Katori, S. Hamada, Y.-W. Lui, R.P. Schmitt, Phys. Lett. B 416 (1998) 43.
- [6] J. Yorkston, A.C. Shotter, T. Davinson, E.W. Macdonald, D. Branford, Nucl. Phys. A 524 (1991) 495.
- [7] S.B. Gazes, J.E. Mason, R.B. Roberts, S.G. Teichmann, Phys. Rev. Lett. 68 (1992) 150.
- [8] J.E. Mason, S.B. Gazes, R.B. Roberts, S.G. Teichmann, Phys. Rev. C 45 (1992) 2870.
- [9] D. Gupta, C. Samanta, R. Kanungo, M.K. Sharan, S. Kailas, A. Chatterjee, K. Mahata, A. Shrivastava, Nucl. Phys. A 646 (1999) 161.
- [10] I. Tanihata, J. Phys. G 22 (1996) 157, see references therein.
- [11] F. Ajzenberg-selove, Nucl. Phys. A 490 (1988) 52.
- [12] Y. Sakuragi, Y. Hirabayashi, in: S. Kubono, T. Kajino (Eds.), Proc. of International Symposium on Origin and Evolution of the Elements, October 1992, Tokyo, World Scientific, Singapore, 1993, p. 220.

- [13] H. Nishioka, J.A. Tostevin, R.C. Johnson, K.-I. Kubo, Nucl. Phys. A 415 (1984) 230.
- [14] I. Martel, J. Gomez-Camacho, K. Rusek, G. Tungate, Nucl. Phys. A 605 (1996) 417.
- [15] K. Rusek, J. Gomez-Camacho, I. Martel-Bravo, G. Tungate, Nucl. Phys. A 614 (1997) 112.
- [16] K. Rusek, C.O. Blyth, N.M. Clarke, P.R. Dee, B.R. Fulton, J.A.R. Griffith, S.J. Hall, N. Keeley, I. Martel-Bravo, G. Tungate, N.J. Davis, K.A. Connell, J.S. Lilley, M.W. Bailey, J. Gomez-Camacho, Nucl. Phys. A 575 (1994) 412.
- [17] N.J. Davis, C.H. Shepherd-Themistocleous, A.C. Shotter, T. Davinson, D.G. Ireland, K. Livingston, E.W. Macdonald, R.D. Page, P.J. Sellin, P.J. Woods, N.M. Clarke, G. Tungate, J.A.R. Griffith, S.J. Hall, O. Karban, I. Martel-Bravo, J.M. Nelson, K. Rusek, J. Gomez-Camacho, Phys. Rev. C 52 (1995) 3201.
- [18] I. Martel, J. Gomez-Camacho, C.O. Blyth, N.M. Clarke, P.R. Dee, B.R. Fulton, J.A.R. Griffith, S.J. Hall, N. Keeley, G. Tungate, N.J. Davis, K. Rusek, K.A. Connell, J.S. Lilley, M.W. Bailey, Nucl. Phys. A 582 (1995) 357.
- [19] N. Keeley, K. Rusek, Phys. Lett. B 427 (1998) 1.
- [20] D. Gupta, C. Samanta, A. Chatterjee, K. Rusek, Y. Hirabayashi, J. Phys. G 26 (2000) L81.
- [21] Y. Sakuragi, M. Yahiro, M. Kamimura, Prog. Theor. Phys. 89 (1986) 136.
- [22] Y. Sakuragi, in: Int. Nucl. Phys. Conf., Harrogate, UK, August 1986.
- [23] S.S. Rattan, A.V.R. Reddy, V.S. Mallapurkar, R.J. Singh, S. Prakash, M.V. Ramaniah, Phys. Rev. C 27 (1983) 327.
- [24] T. Davinson, V. Rapp, A.C. Shotter, D. Branford, M.A. Nagarajan, I.J. Thompson, N.E. Sander-son, Phys. Lett. B 139 (1984) 150.
- [25] P.D. Kunz, computer code DWUCK4, unpublished.
- [26] A.F. Zeller, D.C. Weissner, T.R. Ophel, D.F. Hebbard, Nucl. Phys. A 332 (1979) 515.
- [27] F. Rybicki, N. Austern, Phys. Rev. C 6 (1972) 1525.
- [28] C. Samanta, R. Kanungo, S. Mukherjee, D.N. Basu, Phys. Lett. B 352 (1995) 197.
- [29] C. Samanta, S. Mukherjee, R. Kanungo, D.N. Basu, Phys. Rev. C 53 (1996) 2287.
- [30] J. Cook, At. Nucl. Data Tables 26 (1981) 19.
- [31] Y. Hirabayashi, private communication.
- [32] G.M. Hudson, R.H. Davis, Phys. Rev. C 9 (1974) 1521.
- [33] E.R. Flynn, D.D. Armstrong, J.G. Beery, A.G. Blair, Phys. Rev. 182 (1969) 1113.
- [34] S. Kailas, S.K. Gupta, S. Bhattacharya, S.N. Chintalapudi, Y.P. Viyogi, Pramana 23 (1984) 495.